Improved density-dependent cluster model in α-decay calculations within anisotropic deformation-dependent surface diffuseness

Zhen Wang [1], Dong Bai [2], and Zhongzhou Ren [1,3,*]

[1] *School of Physics Science and Engineering, Tongji University, Shanghai 200092, China*

[2] *College of Science, Hohai University, Nanjing 211100, China*

[3] *Key Laboratory of Advanced Micro-Structure Materials, Ministry of Education, Shanghai 200092, China*

(Received 19 January 2022; accepted 9 February 2022; published 23 February 2022)

The density-dependent cluster model (DDCM) is one of the successful theoretical models for α-decay studies. It gives a good description of the experimental α-decay half-lives for a wide range of α emitters. Nuclear surface diffuseness, one important quantity in determining the nucleon density profiles, is extremely sensitive to deformation, Bohr, Mottelson *et al.* proposed an anisotropic feature of the surface diffuseness for the deformed nuclei. In this work, an improved version of the density-dependent cluster model, abbreviated as DDCM+, is developed to optimize α-decay calculations on half-lives, by accounting for the anisotropy and polarization effects of surface diffuseness due to nuclear deformation. Within a deformation-dependent diffuseness correction, the response of α-decay dynamics to the diffuseness anisotropy is first investigated in detail. It demonstrates that such an anisotropic deformation-dependent diffuseness would change the shape of nucleon density profile and effective α-core interactions, yielding longer calculated α-decay half-lives, as well as suggesting larger estimated α-preformation factors. The systematic calculations on α-decay half-lives are subsequently performed for 157 even-even nuclei with $52 \leqslant Z \leqslant 118$, which reproduce the experimental data within an average factor of 1.88, and drastically reduce the root-mean-square deviations between theoretical results and experimental data by about 41.4% in contrast to conventional DDCM. Noticeably, the theoretical result of new isotope ^{214}U [Zhang *et al.*, Phys. Rev. Lett. **126**, 152502 (2021)] given by DDCM+ also shows good agreement with the latest reported experimental data, demonstrating the high reliability of the improved model. It is expected that this improved model could be useful for future experimental and theoretical studies of α decays.

DOI: 10.1103/PhysRevC.105.024327

I. INTRODUCTION

Probing the nuclear structure is one of the most fundamental tasks in modern nuclear physics. Nowadays, it has been a hot topic to investigate the properties of nuclear surface especially for exotic nuclei far away from the β-stability valley, since the nuclear surface profile could provide abundant valuable information on nuclear structure [1–3]. Specifically, particular attention has been given to the nuclear surface diffuseness, which is a basic quantity characterizing the nuclear surface thickness. Thanks to the advances of radioactive ion beam facilities, in recent years, many exotic structures such as the halos [4–8], skins [9], and bubble-like structure [10], etc., have been discovered. Such exotic structures are dominated by nuclear dynamics around the nuclear surface region, implying there exist complicated and nontrivial behaviors of nuclear surface diffuseness. Moreover, from a microscopic perspective, some studies also indicate that the nuclear surface diffuseness is related to the occupations of nucleons near the Fermi level and strongly sensitive to the deformation [10]. In several previous theoretical works, the investigations on nuclear surface diffuseness are usually restricted to spherical nuclei, however, most nuclei are found to be deformed in their ground state [11], a diffuseness correction is therefore essential for deformed nuclei. In Chap. 4 of Ref. [11], Bohr and Mottelson proposed an anisotropic diffuseness for the deformed system with a correction assuming the gradient of density to be constant at each point of the surface. Based on this argument, Scamps *et al.* gave a systematic and extensive theoretical study on the surface diffuseness of deformed systems, and reported the polarization and anisotropy features of nuclear surface diffuseness [12], which will be also discussed later in Sec. II B. In addition, a similar deformation-dependent diffuseness is also used in Ref. [13], which could well reproduce the equilibrium ground-state deformation of medium and heavy nuclei. All of these studies indicate that the nuclear diffuseness may be anisotropic due to deformation. α decay is one of the dominant decay channels for some unstable nuclei, the nuclear diffuseness is also an important parameter in theoretical α-decay calculations to determine the nuclear density profiles. As most α emitters are deformed, it can be predicted that the diffuseness anisotropy may have a non-negligible impact on α-decay half-lives.

α decay occupies an important position in modern nuclear physics [14–17]. Experimentally, one can identify the new elements and nuclides via observing the position-time correlated α-decay chains from an unknown parent nucleus to its known

*Corresponding author: zren@tongji.edu.cn

 ©2022 American Physical Society

descendants [18–20]. Moreover, the α spectroscopy also provides a powerful tool to probe the nuclear structure properties of heavy and superheavy nuclei [21]. Very recently, a new α-emitter ^{214}U, the hitherto lightest uranium isotope, was synthesized simultaneously with more precise α-decay properties of even-even nuclei $^{216,\,218}$U being measured [18]. Furthermore, the authors of Ref. [18] have revealed that there may exist strong monopole interactions among the valence protons and neutrons occupying the $\pi 1f_{7/2}$ and $\nu 1f_{5/2}$ spin-orbit partner orbits, resulting in an observed enhancement of the α-cluster formation of $^{214,\,216}$U. Also, a series of new nuclides synthesized in recent years are reported in Refs. [22–27]. Despite these achievements, some key nuclides, e.g., ^{220}U, ^{220}Pu, and ^{222}Pu, etc., which are crucial to probe the robustness of the $N = 126$ shell closure, are still unknown in experiments. Besides, the synthesis of superheavy nuclei with $Z > 118$ is also a challenging task [20,28]. Thus, the more accurate and reliable theoretical models for α decay are required for the further synthesis and identification of the unknown nuclei.

From the theoretical side, α decay is interpreted as a quantum tunneling process of a preformed α cluster. Pioneering works on α decay were done by Gamow [29], and independently by Gurney and Condon [30] in 1928, which are regarded as milestones in both nuclear physics and quantum mechanics. Hereafter, various phenomenological and microscopic models have been proposed and developed intensively to explain the observed α-decay experimental data, and provide the quantitative predictions of the α-decay properties for the unknown nuclei, see, e.g., Refs. [31–44] and the papers cited therein, for comprehensive reviews. In Refs. [36–38], the authors proposed and developed a phenomenological model named the density-dependent cluster model (DDCM) with both spherical and deformed versions, which took the nuclear density distribution and the effective nucleon-nucleon interaction into consideration, and reproduced the α-decay half-lives for nuclei in a wide range of $52 \leqslant Z \leqslant 110$, with a great agreement to the experimental data. In addition, DDCM has also been generalized to study the α-cluster structure [43,45] and extract the nuclear charge radii [46,47]. Among these theoretical calculations mentioned above, the surface diffuseness a is mainly performed in two types, i.e., the constant and nonconstant diffuseness. As for the latter case, a fixed constant value is used for all nuclei, e.g., a standard value $a = 0.54$ fm is widely accepted in various calculations, such as the conventional DDCM [36–38]. While for the former case, different values are employed for different nuclei to make the calculations more accurate, such as the isospin dependent diffuseness [48], etc. Nevertheless, one can easily get the insight that both two cases have implicitly assumed an isotropic surface diffuseness for a certain nucleus, without taking the impact of deformation on the diffuseness into consideration. Inspired by the works of Refs. [11–13], it is of great interest to incorporate the anisotropic deformation-dependent diffuseness into conventional DDCM, making the model more realistic.

In this work, we present a new version of DDCM for α decays of deformed nuclei, which improves the conventional model mainly from three aspects: (i) An anisotropic deformation-dependent diffuseness is adopted instead of the isotropic one with a constant value of $a = 0.54$ fm for the deformed α emitters. (ii) A new set of parametrization for half-density radius and nuclear diffuseness is employed in the improved model, where the differences between proton and neutron density distributions are taken into consideration. (iii) Calculating the α-decay half-lives by numerically solving the quasibound Schrödinger equation instead of the two-potential approach combined with Bohr-Sommerfeld quantum condition, to gain a more microscopic insight. The remaining parts of this paper are organized as follows. In Sec. II, we detail the theoretical framework of the improved DDCM, which will be abbreviated as DDCM+ hereafter for convenience. Next, the determination of the deformation-dependent diffuseness and the choice of parametrization are discussed explicitly. In Sec. III, We first look at how α-decay dynamics respond to the newly introduced anisotropic surface diffuseness, the impacts of diffuseness anisotropy on relevant quantities including nucleon density profiles, barrier height and position of α-core effective potential, and quasibound state wave functions are systematically studied. Then we continue to give the numerical results of α decay half-lives for 157 even-even nuclei with $52 \leqslant Z \leqslant 118$, where the α-decay properties of newly discovered isotope ^{214}U and two newly measured nuclei $^{216,\,218}$U are also discussed. Finally, a summary is given in Sec. IV.

II. THEORETICAL FRAMEWORK OF DDCM+ WITH DEFORMATION-DEPENDENT DIFFUSENESS

A. The improved density-dependent cluster model

In the present work, we assume an α emitter to be a binary system of a spherical α cluster interacting with an axially symmetric deformed core nucleus, as shown in Fig. 1. The total interactive potential between α cluster and the core nucleus is composed of mainly three parts, including nuclear, Coulomb, and the centrifugal terms, namely,

$$V(r,\xi) = V_N(r,\xi) + V_C(r,\xi) + \frac{\hbar^2}{2\mu r^2}L(L+1), \qquad (1)$$

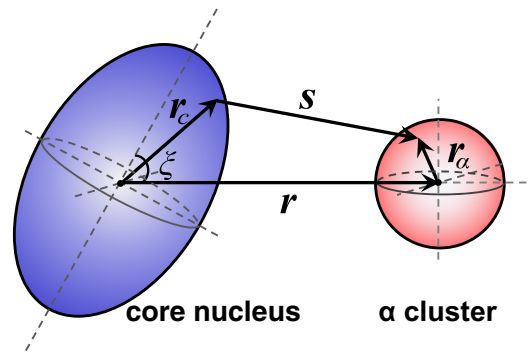

FIG. 1. Schematic illustration of coordinate systems used in the double-folding form interactions between the spherical α cluster and deformed core nucleus. The vector between the center of mass for the core nucleus and α cluster is denoted by $\boldsymbol{r}$, and $\boldsymbol{s}$ represents the vector of relative separation between the two interacting nucleons, whose intrinsic coordinates are respectively denoted by $\boldsymbol{r}_c$ and $\boldsymbol{r}_\alpha$. The letter ξ is the orientation angle between the α-emitting direction and the symmetric axis of the deformed core nucleus.

where ξ is the orientation angle between the α-emitting direction and the symmetric axis of the deformed core nucleus, $\mu = m_\alpha m_c/(m_\alpha + m_c)$ is the reduced mass of α-core system, and L presents the angular momentum carried by the α cluster. Noting that $L = 0$ should be taken for the α decays of even-even nuclei from ground state to ground state.

The analytic expressions of the nuclear potential $V_N(r,\xi)$ and Coulomb interaction $V_C(r,\xi)$, are both written in the double-folding forms as a function of relative distance $r = |\boldsymbol{r}|$ and the orientation angle ξ:

$$V_N(r,\xi) = \lambda \int d\boldsymbol{r}_\alpha \int d\boldsymbol{r}_c \big[\rho_\alpha^p(\boldsymbol{r}_\alpha)+\rho_\alpha^n(\boldsymbol{r}_\alpha)\big]\times\big[\rho_c^p(\boldsymbol{r}_c)+\rho_c^n(\boldsymbol{r}_c)\big] \times v(s = |\boldsymbol{r}_c + \boldsymbol{r} - \boldsymbol{r}_\alpha|) \tag{2}$$

and

$$V_C(r,\xi) = \frac{1}{4\pi\varepsilon_0}\int d\boldsymbol{r}_\alpha \int d\boldsymbol{r}_c \frac{e^2}{s = |\boldsymbol{r}_c + \boldsymbol{r} - \boldsymbol{r}_\alpha|}\rho_\alpha^p(\boldsymbol{r}_\alpha)\rho_c^p(\boldsymbol{r}_c) \tag{3}$$

with λ being the strength factor for the depth of nuclear potential, $\rho_\alpha^{p,n}(\boldsymbol{r}_\alpha)$ and $\rho_c^{p,n}(\boldsymbol{r}_c)$ being the proton (denoted by p) and neutron (denoted by n) density distribution for the α cluster and core nucleus, respectively. $\boldsymbol{r} = (r,\theta,\phi)$ denotes the spherical coordinate, and the azimuth angle ϕ will be implied hereafter due to the axial symmetry of the nucleus. Instead of a fixed value, the strength factor λ will be adjusted to reproduce the experimental α-decay energy Q_α for the quasibound state in subsequent calculations. In Eq. (2), $v(s)$ denotes the effective nucleon-nucleon interaction with $s = |\boldsymbol{r}_c + \boldsymbol{r} - \boldsymbol{r}_\alpha|$ being the relative separation between the two interacting nucleons in the α-core system. Here, the widely used Reid Michigan-3-Yukawa (M3Y) nucleon-nucleon interaction is adopted, which reads

$$\begin{aligned} v(s) &= 7999.00\frac{\exp(-4s)}{4s} - 2134.25\frac{\exp(-2.5s)}{2.5s} \\ &\quad + \hat{J}_{00}(E_\alpha)\delta(s), \\ \hat{J}_{00}(E_\alpha) &= -276(1 - 0.005E_\alpha/A_\alpha). \end{aligned} \tag{4}$$

A simple zero-range pseudopotential $\hat{J}_{00}(E_\alpha)$ is used in Eq. (4) instead of a nonlocal exchange term [49], approximately accounting for the effect of antisymmetrization due to the single-particle knock-on exchange between two interactive nucleons with E_α and A_α representing the kinetic energy and mass number of the emitted α cluster, respectively.

The proton and neutron density distributions for the spherical α cluster are taken to be the standard Gaussian form

$$\rho_\alpha^\tau(\boldsymbol{r}_\alpha) = \rho_\alpha^{\tau_0}\ \exp(-0.7024|\boldsymbol{r}_\alpha|^2) \tag{5}$$

with $\tau_{(0)} = p_{(0)}$ or $n_{(0)}$. As for the core nucleus, we assume the two-parameter Fermi (2pF) distribution for the protons and neutrons,

$$\rho_c^\tau(\boldsymbol{r}_c) = \frac{\rho_c^{\tau_0}}{1+\exp\left[\frac{|\boldsymbol{r}_c|-R^\tau(\theta)}{a^\tau(\theta)}\right]}, \tag{6}$$

where the central densities $\rho_\alpha^{\tau_0}$ and $\rho_c^{\tau_0}$ in Eqs. (5) and (6) can be determined by normalizing the corresponding density distribution to the proton number (or neutron number) of the α cluster and core nucleus, respectively. $R^\tau(\theta)$ and $a^\tau(\theta)$ are, respectively, the half-density radius and surface diffuseness with the elevation angle θ, whose determination will be introduced in Sec. II B.

Based on the aforementioned procedure, instead of using a two-potential approach combined with the Bohr-Sommerfeld condition as in conventional DDCM, here we calculate the α-decay half-lives by numerically solving the quasibound Schrödinger equation. Due to the extreme weakness of the nuclear potential and deformation effect at a large separation distance, the radial wave function $\varphi_L(r,\xi)$ for each certain orientation angle ξ will behave like the spherical outgoing Coulomb wave function as [50,51]

$$\lim_{r\to\infty}\varphi_L(r,\xi) \to N_L[G_L(\eta,kr) + iF_L(\eta,kr)], \tag{7}$$

where N_L denotes a normalization constant, $G_L(\eta,kr)$ and $F_L(\eta,kr)$ are the irregular and regular Coulomb wave function, with $\eta = \mu Z_\alpha Z_c e^2/(4\pi\varepsilon_0\hbar^2 k)$ being the Sommerfeld parameter, and $k = \sqrt{2\mu Q_\alpha}/\hbar$ denoting the wave number, respectively.

In addition, the well-known Wildermuth-Tang condition $G = 2n + L$ is adopted in the calculations to implement the Pauli-blocking effect [51], ensuring that the four nucleons in the α cluster occupy the physically allowed orbits. In this work, the global quantum number G is taken as $G = 22$ for $N > 126$ and $G = 20$ for $82 < N \leqslant 126$. Given the values of G and L, the number of nodes n in the α-cluster radial wave function can then be determined. Subsequently, the orientation-dependent partial α-decay width could be obtained by using the distorted wave approach [21,52]

$$\Gamma(\xi) = \frac{4\mu}{\hbar^2 k}\left|\int_0^\infty F_L(\eta,kr)[V_N(r,\xi)+\delta V_C(r,\xi)]\varphi_L(r,\xi)\,dr\right|^2 \tag{8}$$

with $\delta V_C(r,\xi) = V_C(r,\xi) - Z_\alpha Z_c e^2/(4\pi\varepsilon_0 r)$. The total α-decay width thus can be obtained by integrating the partial decay width along the different orientation

$$\Gamma_\alpha = \int_0^{\frac{\pi}{2}} \Gamma(\xi)\sin\xi\,d\xi. \tag{9}$$

The α-decay half-life $T_{1/2}$ can be then obtained by using the relationship of $T_{1/2} = \hbar\ln 2/(P_\alpha\Gamma_\alpha)$, where P_α is the α-preformation factor, characterizing the probability to form an α cluster on the nuclear surface. Nowadays, it is still a pending problem to calculate the α-preformation factor microscopically. In terms of the fact that P_α is a quantity less than unity and varies smoothly in the open-shell region, we thus take a constant P_α in the present work for the sake of reducing the number of free parameters.

B. The parametrization of deformation-dependent diffuseness

Our main focus in this subsection is the determination of anisotropic surface diffuseness. As shown in Eq. (6), the density profile of core nucleus has the 2pF form factor

$$\hat{f}_\tau(r,\theta) = \frac{1}{1+\exp\left[\frac{r-R^\tau(\theta)}{a^\tau(\theta)}\right]}. \tag{10}$$

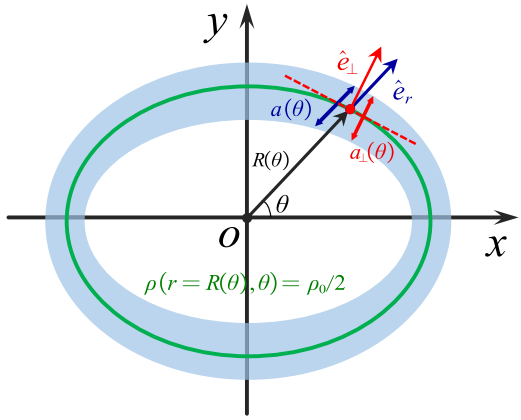

FIG. 2. Comparison of the radial diffuseness $a(\theta)$ (denoted by blue double-side arrow) along the direction of $\hat{e}_r$, and the perpendicular diffuseness $a_\perp(\theta)$ (denoted by red double-side arrow) along the direction of $\hat{e}_\perp$ to the isodensity surface with $\rho(r,\theta) = \rho_0/2$ (denoted by a green solid line).

Inspired by Ref. [11], the deformation of one nucleus can be regarded as the bodily displacement of the surface at each point while maintaining the volume conservation, thus the deformed half-density radius parameter $R^\tau(\theta)$ can be obtained with a rather simple argument that $R^\tau(\theta) = R_0^\tau[1 + \sum_{i=2,4,6}\beta_i Y_{i0}(\theta)]$, with R_0^τ corresponding to the isotropic half-density radius parameter in spherical nuclei, while β_2, β_4, and β_6 being the quadrupole, hexadecapole, and hexacontatetrapole deformation parameters, respectively. Simultaneously, the surface diffuseness is corrected through replacing the isotropic diffuseness parameter a_0^τ in the spherical case by its anisotropic counterpart $a^\tau(\theta)$, with the condition that the gradient of nucleon density form factor at an isodensity surface is constant being respected [11,13]:

$$[\nabla \hat{f}_\tau(r,\theta)]^2_{r=R^\tau(\theta)} = \left[\frac{df_\tau(r)}{dr}\right]^2_{r=R_0^\tau} = \left(-\frac{1}{4a_0^\tau}\right)^2, \tag{11}$$

where $f_\tau(r)$ is the 2pF form factor for the spherical nuclei, with a similar expression as Eq. (10) except that the anisotropic radius $R^\tau(\theta)$ and diffuseness $a^\tau(\theta)$ are replaced by R_0^τ and a_0^τ, respectively. From Eq. (11), one achieves

$$a^\tau(\theta) = a_0^\tau\sqrt{1 + \left[\frac{1}{R^\tau(\theta)}\frac{dR^\tau(\theta)}{d\theta}\right]^2}, \tag{12}$$

the leading order of which just identifies with the original form of the diffuseness correction proposed by Bohr and Mottelson [11].

Such correction in Eq. (12), however, is only valid for weakly deformed nuclei, as discussed in Refs. [11,12]. Further analysis reveals that the isotropic diffuseness a_0^τ in spherical cases actually corresponds to the perpendicular diffuseness $a_\perp^\tau(\theta)$ to the isodensity surface as shown in Fig. 2, which is widely divergent from the radial diffuseness $a^\tau(\theta)$ in the deformed system while they are identical in spherical nuclei. Keeping these points in mind, to overcome the aforementioned limitation of Eq. (12), a more general form of diffuseness correction is adopted in this work:

$$a^\tau(\theta) = a_\perp^\tau(\theta)\sqrt{1 + \left[\frac{1}{R^\tau(\theta)}\frac{dR^\tau(\theta)}{d\theta}\right]^2}, \tag{13}$$

where the effects beyond pure geometric ones are included in the perpendicular diffuseness $a_\perp^\tau(\theta)$, here we refer to Ref. [12] for more details.

In Ref. [12], the authors proposed two sets of parametrizations based on the SKM* and SLy4 energy density functional calculations to describe the nuclear density profiles, however the parametrization sets are not complete, the parametrizations of some key nuclei are not given in their work. To overcome this shortcoming, in the present work, we propose a new form of $a_\perp^\tau(\theta)$ with hexadecapole deformation as

$$a_\perp^\tau(\theta) = a_\perp^{\tau_0}[1 - \beta_2 Y_{20}(\theta)], \tag{14}$$

which could also reproduce the polarization feature of deformed surface described in Ref. [12], without introducing any additional free parameters. Furthermore, $a_\perp^{\tau_0}$ in Eq. (14) can be obtained by averaging the value of anisotropic diffuseness to the corresponding isotropic counterpart with

$$\int_0^{\frac{\pi}{2}} a^\tau(\theta)\sin(\theta)\,d\theta = a_0^\tau. \tag{15}$$

In addition, instead of the standard values in literature, the values of R_0^τ and a_0^τ are estimated in the present work by the São Paulo parametrization with [53]

$$\begin{aligned} R_0^p &= 1.81Z_c^{1/3} - 1.12\ \text{fm}, \quad a_0^p = 0.47 - 0.00083Z_c\ \text{fm}, \\ R_0^n &= 1.49N_c^{1/3} - 0.79\ \text{fm}, \quad a_0^n = 0.47 - 0.00046N_c\ \text{fm}, \end{aligned} \tag{16}$$

respectively, where the differences between proton and neutron density distribution are taken into consideration.

III. NUMERICAL RESULTS AND DISCUSSIONS

A. Impacts of diffuseness anisotropy on α decay dynamics

As discussed in Sec. II, an anisotropic diffuseness is introduced in the improved model DDCM+. Thus, it is of great interest for us to investigate how the anisotropy of surface diffuseness will affect the α-decay dynamics before we perform the theoretical calculations on α-decay half-lives.

Figure 3 illustrates the angular dependences of anisotropic half-density radius (red solid lines) and diffuseness (blue dashed lines), in which the form factors $R^\tau(\theta)/R_0^\tau$ and $a^\tau(\theta)/a_0^\tau$ are presented for one weakly deformed nucleus ^{212}Th, and two well-deformed isotopes ^{204}Ra and ^{238}U, respectively. As can be seen intuitively, the polarization of diffuseness, i.e., the diffuseness tends to reduce along the elongated axis while increasing along the compressed axis, emerges in all the three selected isotopes, which is consistent with the main argument of Ref. [12]. Moreover, such polarization of the diffuseness does not seem to be negligible, here we will take the selected isotope ^{238}U as an example. ^{238}U is a well-deformed nucleus with $|\beta_2| > 0.2$, and an obvious distortion of surface can be seen in panel (c) of Fig. 3. Calculated with Eqs. (13) and (14), the form factor $a^\tau(\theta)/a_0^\tau$ is found to

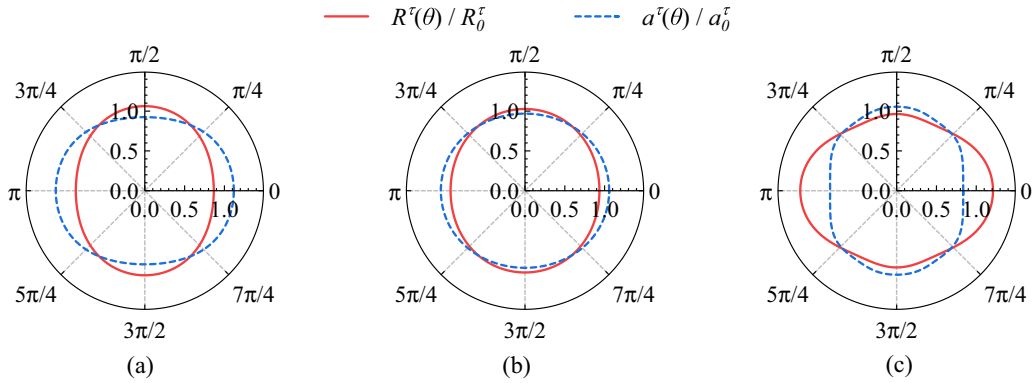

FIG. 3. Form factors of anisotropic half-density radius $R^\tau(\theta)/R_0^\tau$ (red solid lines) and diffuseness $a^\tau(\theta)/a_0^\tau$ (blue dashed lines) as a function of angle θ for (a) ^{204}Ra ($\beta_2 = -0.207$, $\beta_4 = -0.007$, $\beta_6 = 0.003$), (b) ^{212}Th ($\beta_2 = -0.094$, $\beta_4 = -0.008$, $\beta_6 = 0.001$), and (c) ^{238}U ($\beta_2 = 0.236$, $\beta_4 = 0.098$, $\beta_6 = -0.021$), respectively. Noting the polarization of diffuseness are reproduced with Eqs. (13) and (14) for all the three selected isotopes.

vary in a range of 0.837–1.056, which leads to a fluctuation of 21.9% along the half-density isodensity contour with respect to the isotropic diffuseness. In addition, one can further get the insight from Fig. 3 that the fluctuation of diffuseness will be much more significant as the system of larger deformation.

Figure 4(a) presents the nucleon density distribution of ^{238}U, where the polar coordinate (r, θ) is transformed to the Cartesian coordinate (x, y). One can see that the nucleon density is virtually constant in the central region, then decreases steeply to a minor value when it goes far away from the center. Also, in panel (a), the white narrow band is guiding our eyes, which corresponds to the isodensity surface with half-central density, showing the deformation shape of ^{238}U. Considering the non-negligible fluctuation of diffuseness due to the deformation, we then calculate the relative differences between the nucleon density profile calculated by the 2pF distribution with anisotropic $a^\tau(\theta)$ and isotropic diffuseness a_0^τ, which reads

$$\Delta\rho(\boldsymbol{r}) = \rho(\boldsymbol{r})|_{a^\tau(\theta)} - \rho(\boldsymbol{r})|_{a_0^\tau}. \tag{17}$$

In Eq. (17), $R^\tau(\theta)$ are used in both two calculated density profiles, to ensure that any differences of the nucleon density distribution are purely caused by the polarization and anisotropy effects of diffuseness.

In Fig. 4(b), we display a three-dimensional (3D) surface scheme of the nucleon density differences for ^{238}U in the Cartesian coordinate system. In this panel, the z coordinate denotes the value of nucleon density difference. For the sake of clarity, we also depict the projection of the 3D surface to the x-y plane, in which the color map reflects the discrepancies of the nucleon density. Combining Fig. 4(a) with panel (b), one can discover that the nucleon density mainly changes around the surface region, while has minor variation in the central area. What is more, the density differences are positive outside the half-density contour and negative inside it along the compressed axis, whereas the situation is reversed along the elongate axis. This can be easily understood according to Fig. 3(c). Along the compressed axis, the form factor $a^\tau(\theta)/a_0^\tau$ of ^{238}U is greater than unity, implying the density profile with anisotropic diffuseness $a^\tau(\theta)$ is much more extended than that

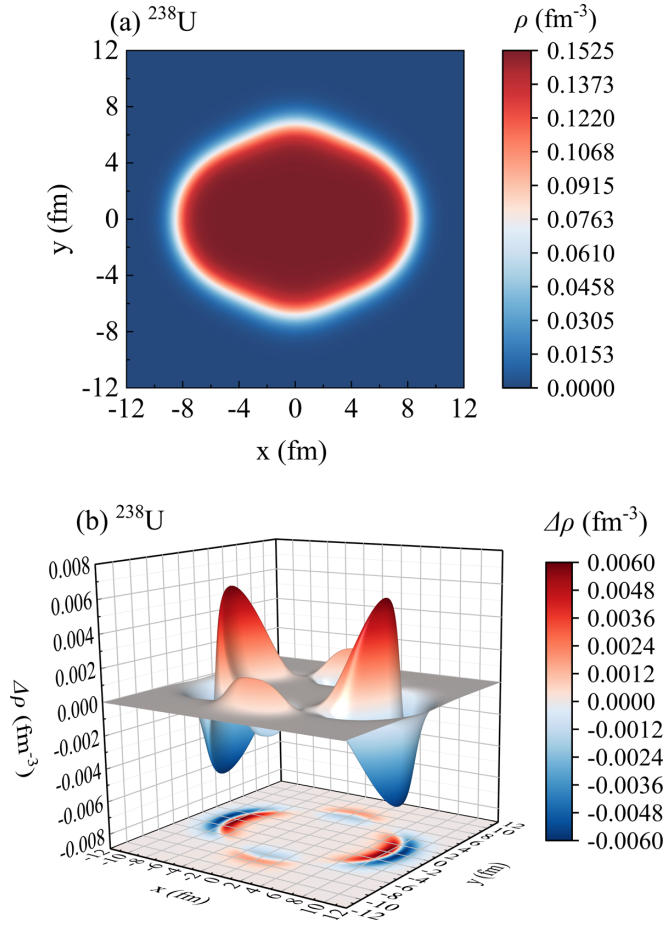

FIG. 4. (a) Nucleon density profiles calculated using 2pF distribution with anisotropic diffuseness for ^{238}U. (b) 3D surface plot of difference between the nucleon density profile respectively calculated using 2pF distribution with anisotropic $a^\tau(\theta)$ and isotropic diffuseness a_0^τ, for selected isotope ^{238}U. Here, $R^\tau(\theta)$ are used in calculations for both cases. Noting the projection of the 3D surface is plotted in x-y plane, where the color map reflects the changes of nucleon density at different points.

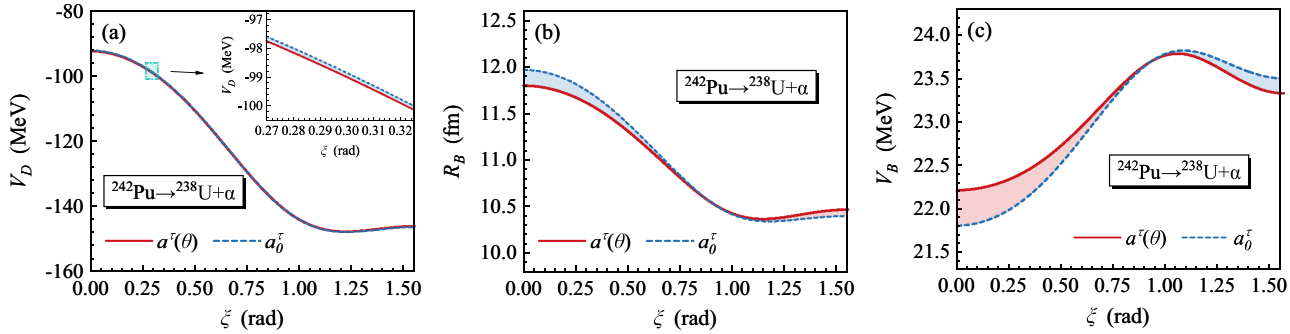

FIG. 5. (a) The depth of inner potential well, (b) the position, and (c) the height of α-core effective potential barrier varying with the orientation angle ξ for the decay channel $^{242}\mathrm{Pu} \rightarrow {}^{238}\mathrm{U}+\alpha$. The theoretical results calculated with anisotropic diffuseness $a^\tau(\theta)$ are denoted by the red solid lines, while ones calculated with isotropic diffuseness a_0^τ are denoted by the blue dashed lines in each panel. We kindly remind the readers here that the orientation angle ξ and the angle θ are different physical quantities in the present models.

one with a_0^τ along this direction, which thus results in a higher density outside the half-density contour and a lower density inside it. Similarly, the situation along the elongate axis could be explained as well.

To figure out the impacts of diffuseness anisotropy and polarization on effective α-core interactions, we show the depth of the inner potential well $V_D(\xi)$, the barrier position $R_B(\xi)$, and barrier height $V_B(\xi)$ versus the orientation angle ξ in Fig. 5(a) to 5(c) for the α decay of $^{242}\mathrm{Pu} \rightarrow {}^{238}\mathrm{U}+\alpha$, for both two cases with $a^\tau(\theta)$ (red solid lines) and a_0^τ (blue dashed lines). Due to the large deformation of ^{238}U, the α-core potential exhibits an obvious dependence on the orientation angle ξ. It can be found that the diffuseness anisotropy has a minor impact on the depth of the inner potential well. However, in contrast to the case with isotropic diffuseness a_0^τ, the geometric shape of the α-core potential barrier is drastically altered by the anisotropy and polarization of diffuseness. As shown, the anisotropic diffuseness brings in a narrower potential well and an increase of potential barrier along with the small orientation angles ξ, whereas it has a reverse situation along with the larger orientation angles.

It is a consensus that the wave functions are closely related to the interactive potentials. Consequently, we plot the radial quasibound wave functions Fig. 6. To show the variations more clearly, we separately plot the internal and exterior wave functions for $\xi = 0$ in panels (a) and (c), as well as plot the cases for $\xi = \pi/2$ in panels (b) and (d). Moreover, we also marked the position and amplitude of the peak for the wave functions in each panel, to present the variations of the wave functions. In the internal region, as the depths of the potential well are nearly identical for both two kinds of diffuseness according to Fig. 5(a), and the nodes of the wave functions are determined by the Wildermuth-Tang condition mentioned in Sec. II A, the internal wave functions are found to be not affected by the diffuseness anisotropy. However, because the penetrability has an exponentially decreasing behavior on the barrier height, significant variations can be observed in exterior wave functions due to the barrier height variations. One can discover from Fig. 6 that the amplitude of the exterior wave function with $a^\tau(\theta)$ is almost 17.5% less than the case with a_0^τ for $\xi = 0$, while it is about 7.6% larger than that for $\xi = \pi/2$. As a result, calculated with $P_\alpha = 1$ temporarily, the DDCM+ gives the theoretical half-life of 2.01×10^{12} s with anisotropic diffuseness $a^\tau(\theta)$, while 1.60×10^{12} s with isotropic diffuseness a_0^τ, which means that the diffuseness anisotropy conducts to an increase of about 25.6% in the α-decay half-life for ^{242}Pu.

B. Numerical results of α-decay half-lives for the observed even-even nuclei with $52 \leqslant Z \leqslant 118$

In this subsection, we perform theoretical calculations on the ground-to-ground state α-decay half-lives of 157 known even-even nuclei from Te to Og by using the improved model DDCM+ introduced in Sec. II. As mentioned in Sec. II A, the α-preformation factor P_α is an important but pending physical quantity up to now. In present theoretical calculations, we approximate the P_α as a constant for considered even-even nuclei via a least-squares fitting approach with 157 experimental half-lives, since the P_α varies smoothly when being far away from the closed-shell region. The yielding constant P_α values for DDCM and DDCM+ are 0.2857 and 0.1521, respectively. As can be seen, there exists a large deviation between the optimized P_α values given by DDCM and DDCM+, which may mainly result from the nucleon-skin thickness and diffuseness anisotropy considered in DDCM+. The former factor has already been investigated in Refs. [21,54], where the authors deduced that the larger neutron or proton thickness would conduct to a lower estimated α-preformation factor P_α. However, the latter factor is not clear up to now. We continue to investigate how the diffuseness anisotropy will affect the P_α values. To have an intuitive scheme, we extract the empirical α-preformation factors along the Th isotopic chain by using DDCM+ with $a^\tau(\theta)$ and a_0^τ, and present the results in Fig. 7. As shown, the P_α values extracted with $a^\tau(\theta)$ are larger than the cases with a_0^τ, the phenomena of which is more significant for the system with larger deformation as moving far away from the $N = 126$ shell closure. According to Fig. 5, it could be deduced that the increase of P_α may result from the additional Coulomb repulsion effect due to diffuseness anisotropy. As mentioned above, the anisotropic diffuseness would optimize the shape of the α-core interaction and give a rise to the Coulomb barrier height along most of the orientations, this additional Coulomb repulsion effect may contribute to the α

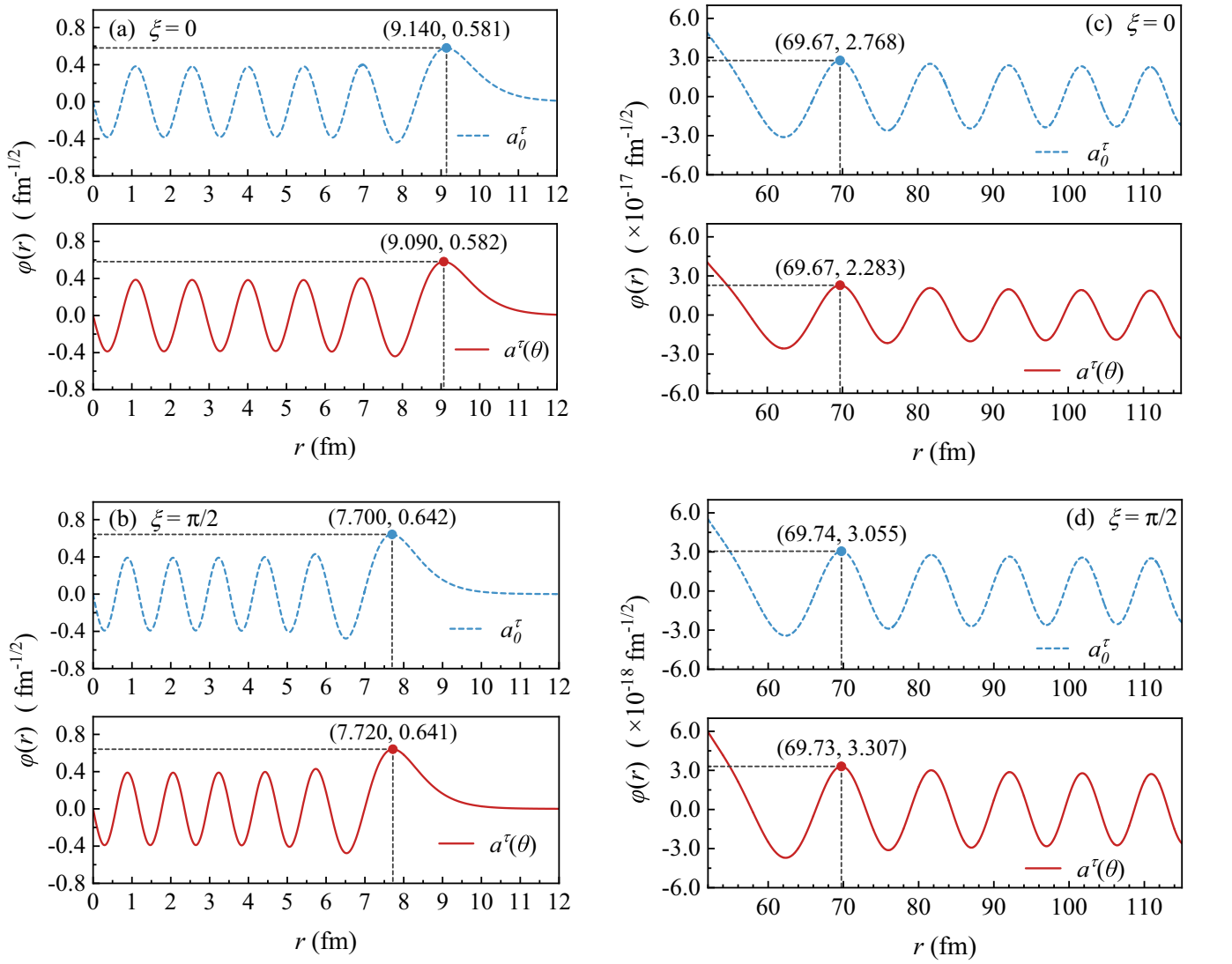

FIG. 6. Comparison of the internal radial wave functions for (a) $\xi = 0$ and (b) $\xi = \pi/2$, as well as the exterior radial wave functions for (c) $\xi = 0$ and (d) $\xi = \pi/2$ between the cases calculated with anisotropic diffuseness $a^\tau(\theta)$ (denoted by red solid lines) and isotropic diffuseness a_0^τ (denoted by blue dashed lines) for the decay channel $^{242}\mathrm{Pu} \rightarrow ^{238}\mathrm{U} + \alpha$.

clustering between the charged α cluster and core nucleus, leading to larger α-preformation factors [55]. Consequently, the large deviation between the optimized P_α values given by DDCM and DDCM+, is a result of competition between the nucleon-thickness effect and Coulomb repulsion effect, where the nucleon-thickness effect dominates here.

Within the deduced P_α values, the numerical results are listed in Table I. The first column represents the α-decay channels. The second column denotes the α-decay energy, the values of which are mainly taken from the AME2020 [56,57]. Columns three to five are the quadrupole, hexadecapole, and hexacontatetrapole deformation parameters taken from the FRDM2012 [58], respectively. The last three columns list the α-decay half-lives in the unit of seconds, with $T_{1/2}^{\mathrm{exp}}$ being the experimental half-lives mainly taken from the NUBASE2020 [59], and $T_{1/2}^{\mathrm{DDCM+}}$ and $T_{1/2}^{\mathrm{DDCM}}$ being the theoretical half-lives given by DDCM+ and DDCM, respectively. Furthermore, it is worth pointing that the nuclei with uncertain or small (<5%) α-decay branching ratios are not included in current calculations.

The experimental half-lives shown in Table I vary in a very wide range from 1.80×10^{-8} s to 2.21×10^{24} s. To see the agreement between the theoretical results and the experimental data, we respectively plot the logarithmic deviations $\delta = \log_{10}(T_{1/2}^{\mathrm{Calc}} / T_{1/2}^{\mathrm{exp}})$ for conventional DDCM and DDCM+ in Fig. 8(a) and 8(b). The blue bands correspond to the deviations within a factor of three. In these years, there are numerous important upgrades in the latest experimental data. As can be straightforwardly seen, the theoretical results given by improved model DDCM+ agree better with these latest experimental data than that of conventional DDCM. For example, in Fig. 8(a) and 8(b), the deviations for three newly measured uranium isotopes ^{214}U, ^{216}U, and ^{218}U [18], are marked by the blue hollow star, triangle, and diamond, respectively. The logarithmic deviations of ^{214}U, ^{216}U, and ^{218}U given by DDCM are 1.053, 0.804, and 0.594, which correspond to the

TABLE I. Calculations on the α-decay half-lives of the deformed nuclei with $52 \leqslant Z \leqslant 118$, from ground state to ground state. In this table, Q_α denotes the α-decay energy taken from Refs. [56,57], β_2, β_4, and β_6 are separately the quadrupole, hexadecapole, and hexacontatetrapole deformation parameters for the daughter nuclei, which are taken from Ref. [58]. $T_{1/2}^{\rm exp}$ denotes the experimental half-lives, while $T_{1/2}^{\rm DDCM+}$ and $T_{1/2}^{\rm DDCM}$ separately denote the theoretical half-lives given by DDCM+ and DDCM. The experimental half-lives are mainly taken from Ref. [59], while the experimental data come from the other references are marked in the first column. The optimized P_α values used in current calculations for DDCM+ and DDCM are 0.1521 and 0.2857, respectively.

α decay	Q_α (MeV)	β_2	β_4	β_6	$T_{1/2}^{\rm exp}$ (s)	$T_{1/2}^{\rm DDCM+}$ (s)	$T_{1/2}^{\rm DDCM}$ (s)
Trans-tin nuclei with $52 \leqslant Z \leqslant 80$, $104 \leqslant A \leqslant 190$							
^{104}Te $\rightarrow$ ^{100}Sn + α [61]	5.100	0.000	0.000	0.000	$<1.80 \times 10^{-8}$	1.06×10^{-7}	9.03×10^{-8}
^{106}Te $\rightarrow$ ^{102}Sn + α	4.290	0.000	0.000	0.000	7.80×10^{-5}	1.70×10^{-4}	9.04×10^{-5}
^{108}Te $\rightarrow$ ^{104}Sn + α	3.420	0.000	0.000	0.000	4.29×10^{0}	8.69×10^{0}	4.63×10^{0}
^{108}Xe $\rightarrow$ ^{104}Te + α	4.569	0.000	0.000	0.000	7.20×10^{-5}	1.17×10^{-4}	6.23×10^{-5}
^{110}Xe $\rightarrow$ ^{106}Te + α	3.872	0.119	0.066	0.018	1.45×10^{-1}	2.66×10^{-1}	1.17×10^{-1}
^{144}Nd $\rightarrow$ ^{140}Ce + α	1.901	0.000	0.000	0.000	7.23×10^{22}	2.91×10^{23}	1.55×10^{23}
^{146}Sm $\rightarrow$ ^{142}Nd + α	2.529	0.000	0.000	0.000	3.25×10^{15}	5.57×10^{15}	2.96×10^{15}
^{148}Sm $\rightarrow$ ^{144}Nd + α	1.987	0.000	0.000	0.000	2.21×10^{23}	6.56×10^{23}	3.49×10^{23}
^{148}Gd $\rightarrow$ ^{144}Sm + α	3.271	0.000	0.000	0.000	2.25×10^{9}	3.47×10^{9}	1.85×10^{9}
^{150}Gd $\rightarrow$ ^{146}Sm + α	2.807	0.000	0.000	0.000	5.65×10^{13}	1.12×10^{14}	5.95×10^{13}
^{152}Gd $\rightarrow$ ^{148}Sm + α	2.204	0.172	0.060	0.009	3.41×10^{21}	7.32×10^{21}	2.87×10^{21}
^{150}Dy $\rightarrow$ ^{146}Gd + α	4.351	0.000	0.000	0.000	1.28×10^{3}	1.40×10^{3}	7.44×10^{2}
^{154}Dy $\rightarrow$ ^{150}Gd + α	2.945	0.172	0.047	0.017	9.47×10^{13}	8.82×10^{13}	3.60×10^{13}
^{152}Er $\rightarrow$ ^{148}Dy + α	4.934	0.011	0.000	0.000	1.14×10^{1}	1.33×10^{1}	1.65×10^{1}
^{154}Yb $\rightarrow$ ^{150}Er + α	5.474	0.011	0.000	0.000	4.42×10^{-1}	4.40×10^{-1}	5.67×10^{-1}
^{156}Hf $\rightarrow$ ^{152}Yb + α	6.026	0.000	0.000	0.000	2.30×10^{-2}	2.17×10^{-2}	1.16×10^{-2}
^{158}Hf $\rightarrow$ ^{154}Yb + α	5.405	−0.104	0.028	0.007	6.43×10^{0}	7.60×10^{0}	1.40×10^{1}
^{174}Hf $\rightarrow$ ^{170}Yb + α [62]	2.494	0.287	−0.018	−0.019	2.21×10^{24}	1.11×10^{24}	6.30×10^{23}
^{158}W $\rightarrow$ ^{154}Hf + α	6.612	0.021	0.000	0.000	1.43×10^{-3}	1.23×10^{-3}	1.71×10^{-3}
^{162}W $\rightarrow$ ^{158}Hf + α	5.678	0.128	0.030	0.003	2.63×10^{0}	3.87×10^{0}	2.78×10^{0}
^{162}Os $\rightarrow$ ^{158}W + α	6.768	0.085	0.003	0.000	2.10×10^{-3}	2.32×10^{-3}	2.61×10^{-3}
^{164}Os $\rightarrow$ ^{160}W + α	6.479	0.128	0.018	0.002	2.19×10^{-2}	2.11×10^{-2}	1.71×10^{-2}
^{166}Os $\rightarrow$ ^{162}W + α	6.143	0.150	0.020	0.002	2.57×10^{-1}	3.58×10^{-1}	2.54×10^{-1}
^{168}Os $\rightarrow$ ^{164}W + α	5.816	0.173	−0.001	−0.001	4.88×10^{0}	7.28×10^{0}	5.43×10^{0}
^{186}Os $\rightarrow$ ^{182}W + α	2.821	0.232	−0.066	−0.006	6.31×10^{22}	4.82×10^{22}	5.35×10^{22}
^{166}Pt $\rightarrow$ ^{162}Os + α	7.292	0.107	−0.008	0.009	2.94×10^{-4}	2.77×10^{-4}	2.97×10^{-4}
^{168}Pt $\rightarrow$ ^{164}Os + α	6.990	0.129	0.006	0.000	2.02×10^{-3}	2.35×10^{-3}	2.17×10^{-3}
^{170}Pt $\rightarrow$ ^{166}Os + α	6.707	0.151	−0.004	−0.001	1.39×10^{-2}	1.98×10^{-2}	1.75×10^{-2}
^{172}Pt $\rightarrow$ ^{168}Os + α	6.463	0.173	−0.013	−0.003	1.02×10^{-1}	1.38×10^{-1}	1.18×10^{-1}
^{174}Pt $\rightarrow$ ^{170}Os + α	6.183	0.184	−0.012	−0.003	1.15×10^{0}	1.54×10^{0}	1.24×10^{0}
^{176}Pt $\rightarrow$ ^{172}Os + α	5.885	0.195	−0.010	−0.003	1.58×10^{1}	2.47×10^{1}	1.86×10^{1}
^{178}Pt $\rightarrow$ ^{174}Os + α	5.573	0.217	−0.007	−0.004	2.69×10^{2}	5.60×10^{2}	3.70×10^{2}
^{190}Pt $\rightarrow$ ^{186}Os + α	3.269	0.209	−0.083	0.003	1.52×10^{19}	7.31×10^{18}	9.90×10^{18}
^{170}Hg $\rightarrow$ ^{166}Pt + α [63]	7.773	−0.105	0.004	0.000	8.00×10^{-5}	5.69×10^{-5}	1.51×10^{-4}
^{172}Hg $\rightarrow$ ^{168}Pt + α	7.524	0.118	0.005	0.000	2.31×10^{-4}	2.85×10^{-4}	2.91×10^{-4}
^{174}Hg $\rightarrow$ ^{170}Pt + α	7.233	0.129	−0.006	−0.001	2.00×10^{-3}	2.15×10^{-3}	2.25×10^{-3}
^{176}Hg $\rightarrow$ ^{172}Pt + α	6.897	0.140	−0.005	−0.001	2.26×10^{-2}	2.65×10^{-2}	2.62×10^{-2}
^{178}Hg $\rightarrow$ ^{174}Pt + α	6.577	0.162	−0.003	−0.001	2.99×10^{-1}	3.40×10^{-1}	2.95×10^{-1}
^{180}Hg $\rightarrow$ ^{176}Pt + α	6.258	0.239	0.021	0.002	5.40×10^{0}	4.39×10^{0}	1.94×10^{0}
^{182}Hg $\rightarrow$ ^{178}Pt + α	5.996	0.250	0.011	−0.001	7.79×10^{1}	5.04×10^{1}	2.35×10^{1}
Trans-lead nuclei with $82 \leqslant Z \leqslant 98$, $178 \leqslant A \leqslant 252$							
^{178}Pb $\rightarrow$ ^{174}Hg + α [64]	7.789	−0.105	−0.019	0.002	2.50×10^{-4}	2.42×10^{-4}	8.07×10^{-4}
^{180}Pb $\rightarrow$ ^{176}Hg + α	7.419	−0.115	−0.030	0.004	4.10×10^{-3}	3.08×10^{-3}	1.23×10^{-2}
^{182}Pb $\rightarrow$ ^{178}Hg + α	7.066	−0.125	−0.017	0.003	5.50×10^{-2}	4.23×10^{-2}	1.71×10^{-1}
^{184}Pb $\rightarrow$ ^{180}Hg + α	6.774	−0.135	−0.005	−0.008	6.13×10^{-1}	4.26×10^{-1}	1.89×10^{0}
^{186}Pb $\rightarrow$ ^{182}Hg + α	6.471	−0.146	−0.004	0.001	1.21×10^{1}	5.60×10^{0}	2.64×10^{1}
^{186}Po $\rightarrow$ ^{182}Pb + α [65]	8.501	0.011	0.000	0.000	3.40×10^{-5}	1.18×10^{-5}	2.11×10^{-5}
^{188}Po $\rightarrow$ ^{184}Pb + α	8.082	0.000	0.012	0.000	2.70×10^{-4}	1.56×10^{-4}	8.30×10^{-5}
^{190}Po $\rightarrow$ ^{186}Pb + α	7.693	0.000	0.000	0.000	2.45×10^{-3}	2.10×10^{-3}	1.12×10^{-3}
^{192}Po $\rightarrow$ ^{188}Pb + α	7.320	0.000	0.000	0.000	3.22×10^{-2}	3.12×10^{-2}	1.66×10^{-2}

TABLE I. (*Continued.*)

α decay	Q_α (MeV)	β_2	β_4	β_6	$T_{1/2}^{\rm exp}$ (s)	$T_{1/2}^{\rm DDCM+}$ (s)	$T_{1/2}^{\rm DDCM}$ (s)
^{194}Po $\rightarrow$ ^{190}Pb + α	6.987	0.000	0.000	0.000	3.92×10^{-1}	4.15×10^{-1}	2.21×10^{-1}
^{196}Po $\rightarrow$ ^{192}Pb + α	6.658	0.000	0.000	0.000	5.99×10^{0}	6.57×10^{0}	3.50×10^{0}
^{198}Po $\rightarrow$ ^{194}Pb + α	6.310	0.000	0.000	0.000	1.85×10^{2}	1.58×10^{2}	8.41×10^{1}
^{208}Po $\rightarrow$ ^{204}Pb + α	5.216	0.000	0.000	0.000	9.15×10^{7}	2.45×10^{7}	1.30×10^{7}
^{210}Po $\rightarrow$ ^{206}Pb + α	5.408	0.000	0.000	0.000	1.20×10^{7}	1.95×10^{6}	1.04×10^{6}
^{212}Po $\rightarrow$ ^{208}Pb + α	8.954	0.000	0.000	0.000	2.94×10^{-7}	1.95×10^{-7}	1.04×10^{-7}
^{214}Po $\rightarrow$ ^{210}Pb + α	7.834	0.000	0.000	0.000	1.63×10^{-4}	1.88×10^{-4}	1.00×10^{-4}
^{216}Po $\rightarrow$ ^{212}Pb + α	6.906	0.000	0.000	0.000	1.44×10^{-1}	2.05×10^{-1}	1.09×10^{-1}
^{218}Po $\rightarrow$ ^{214}Pb + α	6.115	0.000	0.000	0.000	1.86×10^{2}	2.93×10^{2}	1.56×10^{2}
^{194}Rn $\rightarrow$ ^{190}Po + α	7.862	−0.217	0.017	−0.001	7.80×10^{-4}	2.70×10^{-3}	2.58×10^{-2}
^{196}Rn $\rightarrow$ ^{192}Po + α	7.617	−0.217	0.017	−0.001	4.70×10^{-3}	1.48×10^{-2}	1.46×10^{-1}
^{198}Rn $\rightarrow$ ^{194}Po + α	7.349	−0.207	0.015	−0.001	6.92×10^{-2}	1.09×10^{-1}	1.00×10^{0}
^{200}Rn $\rightarrow$ ^{196}Po + α	7.043	0.085	0.003	0.000	1.18×10^{0}	1.49×10^{0}	2.20×10^{0}
^{202}Rn $\rightarrow$ ^{198}Po + α	6.774	0.075	0.002	0.000	1.24×10^{1}	1.44×10^{1}	2.31×10^{1}
^{204}Rn $\rightarrow$ ^{200}Po + α	6.547	−0.063	0.013	−0.001	1.03×10^{2}	1.09×10^{2}	2.87×10^{2}
^{206}Rn $\rightarrow$ ^{202}Po + α	6.384	−0.063	0.001	0.000	5.49×10^{2}	4.83×10^{2}	1.38×10^{3}
^{208}Rn $\rightarrow$ ^{204}Po + α	6.261	−0.042	0.001	0.000	2.36×10^{3}	1.54×10^{3}	3.98×10^{3}
^{210}Rn $\rightarrow$ ^{206}Po + α	6.159	0.000	0.000	0.000	9.00×10^{3}	4.09×10^{3}	2.18×10^{3}
^{212}Rn $\rightarrow$ ^{208}Po + α	6.385	0.000	0.000	0.000	1.43×10^{3}	3.84×10^{2}	2.04×10^{2}
^{214}Rn $\rightarrow$ ^{210}Po + α	9.208	0.000	0.000	0.000	2.59×10^{-7}	2.33×10^{-7}	1.24×10^{-7}
^{216}Rn $\rightarrow$ ^{212}Po + α	8.198	0.000	0.000	0.000	4.50×10^{-5}	9.31×10^{-5}	4.96×10^{-5}
^{218}Rn $\rightarrow$ ^{214}Po + α	7.262	0.000	0.000	0.000	3.38×10^{-2}	7.65×10^{-2}	4.08×10^{-2}
^{220}Rn $\rightarrow$ ^{216}Po + α	6.405	0.000	0.000	0.000	5.56×10^{1}	1.37×10^{2}	7.31×10^{1}
^{222}Rn $\rightarrow$ ^{218}Po + α	5.590	0.056	0.028	0.007	3.30×10^{5}	8.20×10^{5}	1.29×10^{6}
^{202}Ra $\rightarrow$ ^{198}Rn + α [66]	7.880	−0.227	0.019	−0.002	1.60×10^{-2}	1.09×10^{-2}	1.33×10^{-1}
^{204}Ra $\rightarrow$ ^{200}Rn + α	7.637	−0.207	0.004	0.001	6.00×10^{-2}	6.52×10^{-2}	7.17×10^{-1}
^{206}Ra $\rightarrow$ ^{202}Rn + α	7.415	−0.115	0.017	0.008	2.40×10^{-1}	3.95×10^{-1}	1.43×10^{0}
^{208}Ra $\rightarrow$ ^{204}Rn + α	7.273	−0.115	0.017	0.008	1.28×10^{0}	1.15×10^{0}	4.24×10^{0}
^{210}Ra $\rightarrow$ ^{206}Rn + α	7.151	−0.094	0.015	0.009	4.00×10^{0}	3.03×10^{0}	9.69×10^{0}
^{212}Ra $\rightarrow$ ^{208}Rn + α	7.032	−0.063	−0.010	0.001	1.30×10^{1}	8.03×10^{0}	2.58×10^{1}
^{214}Ra $\rightarrow$ ^{210}Rn + α	7.273	0.000	0.000	0.000	2.44×10^{0}	1.00×10^{0}	5.33×10^{-1}
^{216}Ra $\rightarrow$ ^{212}Rn + α	9.526	0.000	0.000	0.000	1.72×10^{-7}	1.99×10^{-7}	1.06×10^{-7}
^{218}Ra $\rightarrow$ ^{214}Rn + α	8.540	0.000	0.000	0.000	2.59×10^{-5}	5.59×10^{-5}	2.97×10^{-5}
^{220}Ra $\rightarrow$ ^{216}Rn + α	7.594	0.000	0.000	0.000	1.81×10^{-2}	3.75×10^{-2}	2.00×10^{-2}
^{222}Ra $\rightarrow$ ^{218}Rn + α	6.678	0.079	0.054	0.012	3.36×10^{1}	6.99×10^{1}	7.22×10^{1}
^{224}Ra $\rightarrow$ ^{220}Rn + α	5.789	0.110	0.068	0.014	3.14×10^{5}	6.11×10^{5}	4.69×10^{5}
^{226}Ra $\rightarrow$ ^{222}Rn + α	4.871	0.110	0.068	0.014	5.05×10^{10}	1.18×10^{11}	9.56×10^{10}
^{208}Th $\rightarrow$ ^{204}Ra + α	8.202	−0.207	−0.007	0.003	2.40×10^{-3}	5.99×10^{-3}	7.63×10^{-2}
^{210}Th $\rightarrow$ ^{206}Ra + α	8.069	−0.125	0.018	0.008	1.60×10^{-2}	1.62×10^{-2}	6.59×10^{-2}
^{212}Th $\rightarrow$ ^{208}Ra + α	7.958	−0.125	0.018	0.008	3.17×10^{-2}	3.34×10^{-2}	1.38×10^{-1}
^{214}Th $\rightarrow$ ^{210}Ra + α	7.827	−0.084	−0.009	0.001	8.70×10^{-2}	8.65×10^{-2}	3.29×10^{-1}
^{216}Th $\rightarrow$ ^{212}Ra + α	8.072	−0.053	−0.011	0.001	2.63×10^{-2}	1.37×10^{-2}	4.21×10^{-2}
^{218}Th $\rightarrow$ ^{214}Ra + α	9.849	0.000	0.000	0.000	1.22×10^{-7}	1.66×10^{-7}	8.82×10^{-8}
^{220}Th $\rightarrow$ ^{216}Ra + α	8.973	0.000	0.000	0.000	1.02×10^{-5}	2.01×10^{-5}	1.07×10^{-5}
^{222}Th $\rightarrow$ ^{218}Ra + α	8.133	0.078	0.054	0.010	2.24×10^{-3}	3.87×10^{-3}	3.94×10^{-3}
^{224}Th $\rightarrow$ ^{220}Ra + α	7.299	0.111	0.081	0.026	1.04×10^{0}	1.67×10^{0}	9.93×10^{-1}
^{226}Th $\rightarrow$ ^{222}Ra + α	6.453	0.122	0.082	0.018	1.84×10^{3}	3.53×10^{3}	2.15×10^{3}
^{228}Th $\rightarrow$ ^{224}Ra + α	5.520	0.143	0.084	0.009	6.04×10^{7}	1.25×10^{8}	7.43×10^{7}
^{230}Th $\rightarrow$ ^{226}Ra + α	4.770	0.164	0.098	0.010	2.38×10^{12}	4.58×10^{12}	2.25×10^{12}
^{232}Th $\rightarrow$ ^{228}Ra + α	4.082	0.174	0.099	0.009	4.42×10^{17}	1.06×10^{18}	5.19×10^{17}
^{214}U $\rightarrow$ ^{210}Th + α [18]	8.696	−0.135	0.007	0.009	5.20×10^{-4}	1.17×10^{-3}	5.87×10^{-3}
^{216}U $\rightarrow$ ^{212}Th + α [18]	8.531	−0.094	−0.008	0.001	2.25×10^{-3}	3.41×10^{-3}	1.43×10^{-2}
^{218}U $\rightarrow$ ^{214}Th + α [18]	8.775	−0.063	−0.022	−0.008	6.50×10^{-4}	6.57×10^{-4}	2.55×10^{-3}
^{222}U $\rightarrow$ ^{218}Th + α	9.481	0.000	0.000	0.000	4.70×10^{-6}	5.12×10^{-6}	2.73×10^{-6}
^{224}U $\rightarrow$ ^{220}Th + α [67]	8.628	0.090	0.055	0.012	8.40×10^{-4}	7.26×10^{-4}	6.71×10^{-4}
^{226}U $\rightarrow$ ^{222}Th + α	7.701	0.111	0.069	0.015	2.69×10^{-1}	4.61×10^{-1}	3.33×10^{-1}

TABLE I. (*Continued.*)

α decay	Q_α (MeV)	β_2	β_4	β_6	$T_{1/2}^{\rm exp}$ (s)	$T_{1/2}^{\rm DDCM+}$ (s)	$T_{1/2}^{\rm DDCM}$ (s)
$^{228}\mathrm{U} \rightarrow {}^{224}\mathrm{Th} + \alpha$	6.800	0.144	0.084	0.010	5.60×10^{2}	8.56×10^{2}	4.76×10^{2}
$^{230}\mathrm{U} \rightarrow {}^{226}\mathrm{Th} + \alpha$	5.992	0.154	0.085	0.010	1.75×10^{6}	3.60×10^{6}	1.95×10^{6}
$^{232}\mathrm{U} \rightarrow {}^{228}\mathrm{Th} + \alpha$	5.414	0.174	0.100	0.011	2.17×10^{9}	3.75×10^{9}	1.67×10^{9}
$^{234}\mathrm{U} \rightarrow {}^{230}\mathrm{Th} + \alpha$	4.858	0.195	0.114	0.022	7.75×10^{12}	8.82×10^{12}	3.10×10^{12}
$^{236}\mathrm{U} \rightarrow {}^{232}\mathrm{Th} + \alpha$	4.573	0.205	0.103	0.010	7.39×10^{14}	1.09×10^{15}	4.31×10^{14}
$^{238}\mathrm{U} \rightarrow {}^{234}\mathrm{Th} + \alpha$	4.270	0.226	0.095	−0.001	1.41×10^{17}	2.74×10^{17}	1.14×10^{17}
$^{228}\mathrm{Pu} \rightarrow {}^{224}\mathrm{U} + \alpha$ [68]	7.940	0.132	0.070	0.006	1.10×10^{0}	4.25×10^{-1}	2.88×10^{-1}
$^{230}\mathrm{Pu} \rightarrow {}^{226}\mathrm{U} + \alpha$	7.178	0.143	0.084	0.009	1.05×10^{2}	1.89×10^{2}	1.07×10^{2}
$^{236}\mathrm{Pu} \rightarrow {}^{232}\mathrm{U} + \alpha$	5.867	0.206	0.116	0.013	9.02×10^{7}	7.02×10^{7}	2.30×10^{7}
$^{238}\mathrm{Pu} \rightarrow {}^{234}\mathrm{U} + \alpha$	5.593	0.215	0.106	0.001	2.77×10^{9}	2.33×10^{9}	8.67×10^{8}
$^{240}\mathrm{Pu} \rightarrow {}^{236}\mathrm{U} + \alpha$	5.256	0.226	0.108	−0.009	2.07×10^{11}	2.20×10^{11}	8.49×10^{10}
$^{242}\mathrm{Pu} \rightarrow {}^{238}\mathrm{U} + \alpha$	4.984	0.236	0.098	−0.021	1.18×10^{13}	1.32×10^{13}	5.93×10^{12}
$^{244}\mathrm{Pu} \rightarrow {}^{240}\mathrm{U} + \alpha$	4.666	0.237	0.086	−0.024	2.57×10^{15}	2.61×10^{15}	1.37×10^{15}
$^{234}\mathrm{Cm} \rightarrow {}^{230}\mathrm{Pu} + \alpha$	7.365	0.195	0.114	0.022	1.93×10^{2}	1.28×10^{2}	3.86×10^{1}
$^{236}\mathrm{Cm} \rightarrow {}^{232}\mathrm{Pu} + \alpha$	7.067	0.206	0.116	0.013	2.27×10^{3}	1.70×10^{3}	5.18×10^{2}
$^{240}\mathrm{Cm} \rightarrow {}^{236}\mathrm{Pu} + \alpha$	6.398	0.215	0.106	0.001	2.63×10^{6}	1.38×10^{6}	4.96×10^{5}
$^{242}\mathrm{Cm} \rightarrow {}^{238}\mathrm{Pu} + \alpha$	6.216	0.226	0.095	−0.012	1.41×10^{7}	1.06×10^{7}	4.42×10^{6}
$^{244}\mathrm{Cm} \rightarrow {}^{240}\mathrm{Pu} + \alpha$	5.902	0.237	0.086	−0.024	5.71×10^{8}	4.30×10^{8}	2.08×10^{8}
$^{246}\mathrm{Cm} \rightarrow {}^{242}\mathrm{Pu} + \alpha$	5.475	0.237	0.073	−0.027	1.49×10^{11}	1.18×10^{11}	6.86×10^{10}
$^{248}\mathrm{Cm} \rightarrow {}^{244}\mathrm{Pu} + \alpha$	5.162	0.237	0.061	−0.030	1.20×10^{13}	1.12×10^{13}	7.83×10^{12}
$^{240}\mathrm{Cf} \rightarrow {}^{236}\mathrm{Cm} + \alpha$	7.711	0.215	0.106	0.001	4.09×10^{1}	3.95×10^{1}	1.32×10^{1}
$^{242}\mathrm{Cf} \rightarrow {}^{238}\mathrm{Cm} + \alpha$	7.517	0.226	0.095	−0.012	3.42×10^{2}	2.07×10^{2}	7.99×10^{1}
$^{244}\mathrm{Cf} \rightarrow {}^{240}\mathrm{Cm} + \alpha$	7.329	0.237	0.085	−0.014	1.55×10^{3}	1.02×10^{3}	4.12×10^{2}
$^{246}\mathrm{Cf} \rightarrow {}^{242}\mathrm{Cm} + \alpha$	6.862	0.237	0.086	−0.024	1.29×10^{5}	8.17×10^{4}	3.80×10^{4}
$^{248}\mathrm{Cf} \rightarrow {}^{244}\mathrm{Cm} + \alpha$	6.361	0.249	0.063	−0.029	2.88×10^{7}	1.67×10^{7}	9.70×10^{6}
$^{250}\mathrm{Cf} \rightarrow {}^{246}\mathrm{Cm} + \alpha$	6.129	0.249	0.051	−0.032	4.13×10^{8}	2.44×10^{8}	1.70×10^{8}
$^{252}\mathrm{Cf} \rightarrow {}^{248}\mathrm{Cm} + \alpha$	6.217	0.250	0.039	−0.035	8.61×10^{7}	8.21×10^{7}	6.71×10^{7}
Trans-fermium nuclei with $100 \leqslant Z \leqslant 118$, $246 \leqslant A \leqslant 294$							
$^{246}\mathrm{Fm} \rightarrow {}^{242}\mathrm{Cf} + \alpha$	8.379	0.237	0.073	−0.027	1.65×10^{0}	1.26×10^{0}	6.30×10^{-1}
$^{248}\mathrm{Fm} \rightarrow {}^{244}\mathrm{Cf} + \alpha$	7.995	0.249	0.063	−0.029	3.45×10^{1}	2.28×10^{1}	1.21×10^{1}
$^{250}\mathrm{Fm} \rightarrow {}^{246}\mathrm{Cf} + \alpha$	7.557	0.249	0.051	−0.032	1.86×10^{3}	8.87×10^{2}	5.71×10^{2}
$^{252}\mathrm{Fm} \rightarrow {}^{248}\mathrm{Cf} + \alpha$	7.154	0.250	0.039	−0.035	9.14×10^{4}	3.48×10^{4}	2.70×10^{4}
$^{254}\mathrm{Fm} \rightarrow {}^{250}\mathrm{Cf} + \alpha$	7.307	0.250	0.027	−0.037	1.17×10^{4}	7.77×10^{3}	7.07×10^{3}
$^{256}\mathrm{Fm} \rightarrow {}^{252}\mathrm{Cf} + \alpha$	7.025	0.251	0.014	−0.030	1.16×10^{5}	1.10×10^{5}	1.08×10^{5}
$^{252}\mathrm{No} \rightarrow {}^{248}\mathrm{Fm} + \alpha$	8.549	0.249	0.051	−0.032	3.65×10^{0}	1.79×10^{0}	1.12×10^{0}
$^{254}\mathrm{No} \rightarrow {}^{250}\mathrm{Fm} + \alpha$	8.226	0.250	0.039	−0.035	5.69×10^{1}	2.01×10^{1}	1.52×10^{1}
$^{256}\mathrm{No} \rightarrow {}^{252}\mathrm{Fm} + \alpha$	8.582	0.250	0.027	−0.037	2.93×10^{0}	1.28×10^{0}	1.12×10^{0}
$^{256}\mathrm{Rf} \rightarrow {}^{252}\mathrm{No} + \alpha$	8.926	0.250	0.027	−0.037	2.13×10^{0}	6.34×10^{-1}	5.50×10^{-1}
$^{258}\mathrm{Rf} \rightarrow {}^{254}\mathrm{No} + \alpha$	9.196	0.251	0.015	−0.040	2.55×10^{-1}	9.21×10^{-2}	9.38×10^{-2}
$^{260}\mathrm{Sg} \rightarrow {}^{256}\mathrm{Rf} + \alpha$	9.901	0.252	0.002	−0.033	1.71×10^{-2}	5.01×10^{-3}	5.33×10^{-3}
$^{264}\mathrm{Hs} \rightarrow {}^{260}\mathrm{Sg} + \alpha$ [69]	10.591	0.242	−0.024	−0.038	1.00×10^{-3}	3.84×10^{-4}	6.17×10^{-4}
$^{266}\mathrm{Hs} \rightarrow {}^{262}\mathrm{Sg} + \alpha$	10.346	0.243	−0.037	−0.031	3.95×10^{-3}	1.45×10^{-3}	2.51×10^{-3}
$^{268}\mathrm{Hs} \rightarrow {}^{264}\mathrm{Sg} + \alpha$ [70]	9.623	0.232	−0.052	−0.023	3.80×10^{-1}	1.22×10^{-1}	2.51×10^{-1}
$^{270}\mathrm{Hs} \rightarrow {}^{266}\mathrm{Sg} + \alpha$ [71]	9.070	0.232	−0.052	−0.023	7.60×10^{0}	4.99×10^{0}	1.08×10^{1}
$^{270}\mathrm{Ds} \rightarrow {}^{266}\mathrm{Hs} + \alpha$	11.117	0.232	−0.052	−0.023	2.05×10^{-4}	8.30×10^{-5}	1.66×10^{-4}
$^{282}\mathrm{Ds} \rightarrow {}^{278}\mathrm{Hs} + \alpha$ [72]	8.960	0.130	−0.042	−0.005	6.70×10^{1}	5.85×10^{1}	1.94×10^{2}
$^{286}\mathrm{Cn} \rightarrow {}^{282}\mathrm{Ds} + \alpha$	9.235	0.130	−0.043	0.005	3.00×10^{1}	3.84×10^{1}	1.24×10^{2}
$^{286}\mathrm{Fl} \rightarrow {}^{282}\mathrm{Cn} + \alpha$	10.355	0.086	−0.009	−0.011	2.03×10^{-1}	1.24×10^{-1}	4.27×10^{-1}
$^{288}\mathrm{Fl} \rightarrow {}^{284}\mathrm{Cn} + \alpha$	10.076	0.086	−0.021	−0.002	6.53×10^{-1}	6.69×10^{-1}	2.43×10^{0}
$^{290}\mathrm{Fl} \rightarrow {}^{286}\mathrm{Cn} + \alpha$ [72]	9.856	0.075	−0.034	0.008	2.10×10^{1}	2.66×10^{0}	1.08×10^{1}
$^{290}\mathrm{Lv} \rightarrow {}^{286}\mathrm{Fl} + \alpha$	10.997	0.064	−0.010	−0.001	9.00×10^{-3}	1.16×10^{-2}	4.33×10^{-2}
$^{292}\mathrm{Lv} \rightarrow {}^{288}\mathrm{Fl} + \alpha$	10.791	−0.021	0.012	0.000	1.60×10^{-2}	3.69×10^{-2}	1.77×10^{-1}
$^{294}\mathrm{Og} \rightarrow {}^{290}\mathrm{Lv} + \alpha$	11.867	0.064	−0.022	−0.001	7.00×10^{-4}	3.82×10^{-4}	1.56×10^{-3}

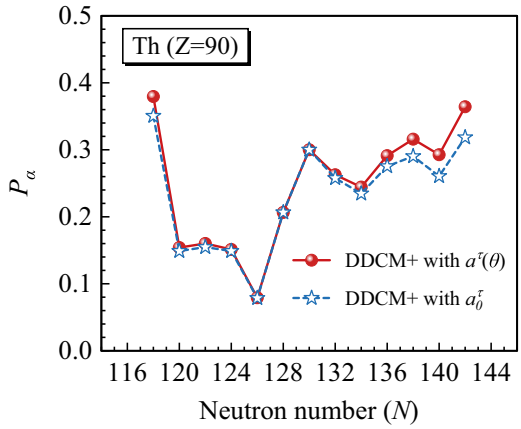

FIG. 7. The extracted α-preformation factors P_α along Th isotopic chain by using DDCM+ with anisotropic diffuseness $a^\tau(\theta)$ and isotropic diffuseness a_0^τ, which are denoted by red spheres with solid lines and blue hollow stars with dashed lines, respectively.

factors of 11.293, 6.368, and 3.925, respectively. However, as for the cases with DDCM+, the logarithmic deviations reduce to 0.352, 0.181, and 0.0045, indicating that the theoretical α-decay half-lives given by DDCM+ are in good accordance with the experimental data with the factors of 2.248, 1.517, and 1.010, respectively. Within the DDCM+, the logarithmic deviations have been significantly reduced by almost 66.58%, 77.49%, and 99.24%, respectively. All of these show that the DDCM+ is a pretty good model for describing the α-decay properties.

Though the theoretical results given by DDCM+ agree with the experimental data very well, one can see that there still exist some nuclei where data deviate far from the experimental data, such as ^{290}Fl marked in Fig. 8(b). There is a maximum logarithmic deviation of -0.897 for ^{290}Fl, which may be due to the inaccurate experimental data. One could find that the experimental data of ^{290}Fl is marked by "tentative" in the original literature [72], consequently, the result may be improved with the more accurate experimental data in the future. As well, the larger deviations can be seen for the nuclei around the $N = 126$ closed shell in both panels, the reason for this is because the constant P_α does not include the structure effect, such as shell effects. Similarly, the large deviation for ^{104}Te may also result from this reason. The nuclide ^{104}Te is near the $N = Z = 50$ closed shells, the authors of Ref. [61] deduced that it has a superallowed α-decay mode, where the constant P_α used in this work has obviously underestimated the α-preformation factor. This issue can be surmounted by varying the P_α values for different α emitters [33,60], one study on the α decays of nuclei in the vicinity of $N = 126$ shell closure can be found in our previous work in Ref. [33].

Furthermore, to systematically evaluate the agreements between the theoretical half-lives and experimental data, we also calculate the root-mean-square (rms) deviation

$$\sigma = \sqrt{\sum_{i=1}^{N_T} \left[\log_{10}\left(T_{1/2}^{\mathrm{Calc},\,i}/T_{1/2}^{\mathrm{exp},\,i}\right)\right]^2 / N_T}, \qquad (18)$$

where i denotes the ith nuclei, N_T is the total number of nuclei included in present calculations. The rms deviation for the conventional DDCM is 0.4666, whereas the rms deviation is reduced to 0.2734 for the improved model DDCM+. The results show that, within the anisotropic diffuseness correction and other improvements, the DDCM+ gives theoretical half-lives in much better agreements with experimental data.

IV. SUMMARY

In this work, we present an improved version of the density-dependent cluster model (DDCM) named DDCM+, which takes into account the diffuseness polarization and anisotropy effects, as well as the differences between proton and neutron density distributions. Moreover, the distort wave approach with solving the quasibound state wave function is also employed in the calculations of α-decay width, to gain a more microscopic insight on α decay. Within the framework of DDCM+, we first investigate the impacts of diffuseness polarization and anisotropy on α-decay dynamics. It shows that such a nontrivial distorted behavior of diffuseness mainly

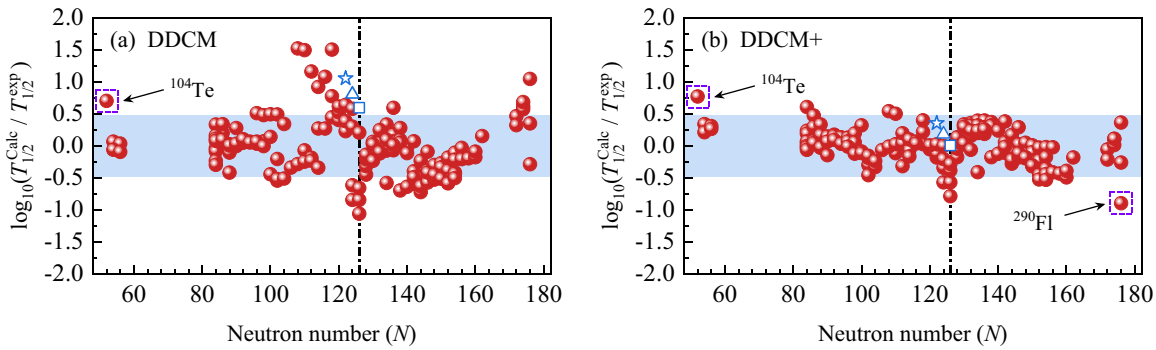

FIG. 8. The logarithmic deviations between the theoretical calculations and the experimental data with (a) conventional DDCM and (b) DDCM+ versus the neutron numbers of daughter nuclei. Remarkably, the blue hollow star, triangle, and square in each panel denote the logarithmic deviations for new isotopes ^{214}U, ^{216}U, and ^{218}U, respectively. The blue band in each panel denotes that the theoretical model reproduces the α-decay half-lives with a factor of three in this region, while the dotted-dashed lines denote the neutron number of $N = 126$. The DDCM+ significantly reduces the rms deviation by about 41.4%.

affects the density profile around the nuclear surface, whereas hardly has any influence on the central density. The modified density profile optimizes the shape of α-core effective interactions, which brings a stronger Coulomb repulsion effect, leading to a larger estimated α-preformation factor and a longer half-life.

Then, we further use the DDCM+ to study the α-decay half-lives for 157 even-even nuclei, located in the medium, heavy, and superheavy mass regions, respectively. The theoretical results given by DDCM+ are in good accordance with the latest experimental data yielding a rms deviation of 0.2734, which is about 41.4% less than the rms deviation of DDCM. This indicates a very significant improvement in half-life calculations. Particularly, the theoretical results of one newly synthesized isotope ^{214}U and two newly measured nuclei $^{216,\ 218}$U given by DDCM+ also shows better agreement with the latest reported experimental data than conventional DDCM, with a factor of 2.248, 1.517, and 1.010, respectively. All of these show that the DDCM+ is indeed a reliable theoretical model for α-decay studies.

The improved model DDCM+ provides a more accurate estimation on α decay half-lives and can be easily generalized to the cases of odd-A and odd-odd nuclei. It is expected that the present work can serve as a useful reference for the identification of new nuclides or elements in the future.

ACKNOWLEDGMENTS

This work is supported by the National Natural Science Foundation of China (Grants No. 12035011, 11975167, 11535004, 11947211, 11905103, 11761161001, 11375086, 11565010, 11881240623, and 11961141003), by the National Key R&D Program of China (Contracts No. 2018YFA0404403 and2016YFE0129300), by the Science and Technology Development Fund of Macau under Grant No. 008/2017/AFJ, by the Fundamental Research Funds for the Central Universities (Grant No. 22120200101).

[1] M. Tanaka, M. Takechi, A. Homma, M. Fukuda *et al.*, Phys. Rev. Lett. **124**, 102501 (2020).
[2] V. Choudhary, W. Horiuchi, M. Kimura, and R. Chatterjee, Phys. Rev. C **102**, 034619 (2020).
[3] S. Hatakeyama, W. Horiuchi, and A. Kohama, Phys. Rev. C **97**, 054607 (2018).
[4] I. Tanihata, H. Savajols, and R. Kanungo, Prog. Part. Nucl. Phys. **68**, 215 (2013).
[5] W. Mittig, J. M. Chouvel, Z. W. Long, L. Bianchi, A. Cunsolo, B. Fernandez, A. Foti, J. Gastebois, A. Gillibert, C. Gregoire *et al.*, Phys. Rev. Lett. **59**, 1889 (1987).
[6] Z. Ren, B. Chen, Z. Ma, and G. Xu, Phys. Rev. C **53**, R572 (1996).
[7] M. V. Zhukov, B. V. Danilin, D. V. Fedorov, J. M. Bang, I. J. Thompson, and J. S. Vaagen, Phys. Rep. **231**, 151 (1993).
[8] B. A. Brown and P. G. Hansen, Phys. Lett. B **381**, 391 (1996).
[9] D. Adhikari *et al.*, Phys. Rev. Lett. **126**, 172502 (2021).
[10] V. Choudhary, W. Horiuchi, M. Kimura, and R. Chatterjee, Phys. Rev. C **104**, 054313 (2021).
[11] A. Bohr and B. Mottelson, *Nuclear Structure Vol. 2: Nuclear Deformations* (World Scientific, Singapore, 1998).
[12] G. Scamps, D. Lacroix, G. G. Adamian, and N. V. Antonenko, Phys. Rev. C **88**, 064327 (2013).
[13] G. I. Bykhalo, V. N. Orlin, and K. A. Stopani, arXiv:2107.08245 [nucl-th].
[14] R. G. Lovas, R. J. Liotta, A. Insolia, K. Varga, and D. S. Delion, Phys. Rep. **294**, 265 (1998).
[15] D. S. Delion, Z. Ren, A. Dumitrescu, and D. Ni, J. Phys. G **45**, 053001 (2018).
[16] S. Peltonen, D. S. Delion, and J. Suhonen, Phys. Rev. C **78**, 034608 (2008).
[17] C. Qi, R. Liotta, and R. Wyss, Prog. Part. Nucl. Phys. **105**, 214 (2019).
[18] Z. Y. Zhang, H. B. Yang, M. H. Huang *et al.*, Phys. Rev. Lett. **126**, 152502 (2021).
[19] Z. Ren and B. Zhou, Front. Phys. (Beijing) **13**, 132110 (2018).
[20] S. A. Giuliani, Z. Matheson, W. Nazarewicz, E. Olsen, P.-G. Reinhard, J. Sadhukhan, B. Schuetrumpf, N. Schunck, and P. Schwerdtfeger, Rev. Mod. Phys. **91**, 011001 (2019).
[21] D. Ni and Z. Ren, Phys. Rev. C **92**, 054322 (2015).
[22] H. B. Yang, L. Ma, Z. Y. Zhang *et al.*, Phys. Lett. B **777**, 212 (2018).
[23] Z. Y. Zhang, Z. G. Gan, H. B. Yang *et al.*, Phys. Rev. Lett. **122**, 192503 (2019).
[24] L. Ma, Z. Y. Zhang, Z. G. Gan *et al.*, Phys. Rev. Lett. **125**, 032502 (2020).
[25] M. D. Sun, Z. Liu, T. H. Huang *et al.*, Phys. Lett. B **771**, 303 (2017).
[26] T. H. Huang, W. Q. Zhang, M. D. Sun *et al.*, Phys. Rev. C **98**, 044302 (2018).
[27] J. L. Pore, J. M. Gates, R. Orford *et al.*, Phys. Rev. Lett. **124**, 252502 (2020).
[28] M. Ismail and A. Adel, Phys. Rev. C **101**, 024607 (2020).
[29] G. Gamow, Z. Phys. **51**, 204 (1928).
[30] R. Gurney and E. Condon, Nature (London) **122**, 439 (1928).
[31] B. A. Brown, Phys. Rev. C **46**, 811 (1992).
[32] B. Buck, A. C. Merchant, and S. M. Perez, Phys. Rev. C **45**, 2247 (1992).
[33] Z. Wang, Z. Ren, and D. Bai, Phys. Rev. C **101**, 054310 (2020).
[34] K. Varga, R. G. Lovas, and R. J. Liotta, Phys. Rev. Lett. **69**, 37 (1992).
[35] G. Royer, Nucl. Phys. A **848**, 279 (2010).
[36] C. Xu and Z. Ren, Nucl. Phys. A **753**, 174 (2005).
[37] C. Xu and Z. Ren, Phys. Rev. C **73**, 041301(R) (2006).
[38] C. Xu and Z. Ren, Phys. Rev. C **74**, 014304 (2006).
[39] P. Mohr, Phys. Rev. C **73**, 031301(R) (2006).
[40] V. Yu. Denisov, O. I. Davidovskaya, and I. Yu. Sedykh, Phys. Rev. C **92**, 014602 (2015).
[41] S. Yang, C. Xu, and G. Röpke, Phys. Rev. C **104**, 034302 (2021).
[42] D. Bai, Z. Ren, and G. Röpke, Phys. Rev. C **99**, 034305 (2019).
[43] D. Bai and Z. Ren, Phys. Rev. C **103**, 044316 (2021).
[44] J. G. Deng, J. C. Zhao, P. C. Chu, and X. H. Li, Phys. Rev. C **97**, 044322 (2018).
[45] D. Ni and Z. Ren, Phys. Rev. C **83**, 014310 (2011).
[46] D. Ni, Z. Ren, T. Dong, and Y. Qian, Phys. Rev. C **87**, 024310 (2013).
[47] Y. Qian, Z. Ren, and D. Ni, Phys. Rev. C **89**, 024318 (2014).
[48] Y. Qian and Z. Ren, J. Phys. G **43**, 065102 (2016).

[49] J. E. Perez Velasquez, N. G. Kelkar, and N. J. Upadhyay, Phys. Rev. C **99**, 024308 (2019).
[50] R. M. Devries, Comput. Phys. Commun. **11**, 249 (1976).
[51] D. Ni and Z. Ren, Phys. Rev. C **80**, 051303(R) (2009).
[52] C. N. Davids and H. Esbensen, Phys. Rev. C **61**, 054302 (2000).
[53] L. C. Chamon, B. V. Carlson, L. R. Gasques, D. Pereira, C. De Conti, M. A. G. Alvarez, M. S. Hussein, M. A. Candido Ribeiro, E. S. Rossi, Jr., and C. P. Silva, Phys. Rev. C **66**, 014610 (2002).
[54] W. M. Seif and A. Abdurrahman, Chin. Phys. C **42**, 014106 (2018).
[55] N. Wan and J. Fan, Phys. Rev. C **104**, 064320 (2021).
[56] W. J. Huang, M. Wang, F. G. Kondev, G. Audi, and S. Naimi, Chin. Phys. C **45**, 030002 (2021).
[57] M. Wang, W. J. Huang, F. G. Kondev, G. Audi, and S. Naimi, Chin. Phys. C **45**, 030003 (2021).
[58] P. Möller, A. J. Sierk, T. Ichikawa, and H. Sagawa, At. Data Nucl. Data Tables **109–110**, 1 (2016).
[59] F. G. Kondev, M. Wang, W. J. Huang, S. Naimi, and G. Audi, Chin. Phys. C **45**, 030001 (2021).
[60] D. Deng and Z. Ren, Phys. Rev. C **93**, 044326 (2016).
[61] K. Auranen, D. Seweryniak, M. Albers, A. D. Ayangeakaa, S. Bottoni, M. P. Carpenter, C. J. Chiara, P. Copp, H. M. David, D. T. Doherty *et al.*, Phys. Rev. Lett. **121**, 182501 (2018).
[62] V. Caracciolo, S. Nagorny, P. Belli, R. Bernabei, F. Cappella, R. Cerulli, A. Incicchitti, M. Laubenstein, V. Merlo, S. Nisi *et al.*, Nucl. Phys. A **1002**, 121941 (2020).
[63] J. Hilton, J. Uusitalo, J. Sarén, R. D. Page, D. T. Joss, M. A. M. AlAqeel, H. Badran, A. D. Briscoe, T. Calverley, D. M. Cox *et al.*, Phys. Rev. C **100**, 014305 (2019).
[64] H. Badran, C. Scholey, K. Auranen, T. Grahn, P. T. Greenlees, A. Herzan, U. Jakobsson, R. Julin, S. Juutinen, J. Konki *et al.*, Phys. Rev. C **94**, 054301 (2016).
[65] A. N. Andreyev, M. Huyse, P. Van Duppen, C. Qi, R. J. Liotta, S. Antalic, D. Ackermann, S. Franchoo, F. P. Heßberger, S. Hofmann *et al.*, Phys. Rev. Lett. **110**, 242502 (2013).
[66] J. Uusitalo, M. Leino, T. Enqvist, K. Eskola, T. Grahn, P. T. Greenlees, P. Jones, R. Julin, S. Juutinen, A. Keenan *et al.*, Phys. Rev. C **71**, 024306 (2005).
[67] S. Singh and B. Singh, Nucl. Data Sheets **130**, 127 (2015).
[68] K. Nishio, H. Ikezoe, S. Mitsuoka, K. Satou, and C. J. Lin, Phys. Rev. C **68**, 064305 (2003).
[69] N. Sato, H. Haba, T. Ichikawa *et al.*, J. Phys. Soc. Jpn. **80**, 094201 (2011).
[70] K. Nishio, S. Hofmann, F. P. Hessberger, D. Ackermann, S. Antalic, Y. Aritomo, V. F. Comas, C. E. Dullmann, A. Gorshkov, R. Graeger *et al.*, Phys. Rev. C **82**, 024611 (2010).
[71] Y. T. Oganessian, V. K. Utyonkov, F. Sh. Abdullin, S. N. Dmitriev, R. Graeger, R. A. Henderson, M. G. Itkis, Yu. V. Lobanov, A. N. Mezentsev, K. J. Moody *et al.*, Phys. Rev. C **87**, 034605 (2013).
[72] S. Hofmann, S. Heinz, R. Mann, J. Maurer, G. Münzenberg, S. Antalic, W. Barth, H. G. Burkhard, L. Dahl, K. Eberhardt *et al.*, Eur. Phys. J. A **52**, 180 (2016).